ENVIRONMENTAL RESEARCH
LETTERS

LETTER • OPEN ACCESS

Rain-on-snow events in Alaska, their frequency and distribution from satellite observations

To cite this article: Caleb G Pan *et al* 2018 *Environ. Res. Lett.* **13** 075004

Environmental Research Letters

OPEN ACCESS

RECEIVED
24 February 2018

REVISED
25 May 2018

ACCEPTED FOR PUBLICATION
4 June 2018

PUBLISHED
28 June 2018

LETTER

Rain-on-snow events in Alaska, their frequency and distribution from satellite observations

Caleb G Pan[1,2,4], Peter B Kirchner[1,3], John S Kimball[1,2], Youngwook Kim[1,2] and Jinyang Du[1,2]

[1] WA Franke College of Forestry and Conservation, University of Montana, Missoula, MT, United States of America
[2] Numerical Terradynamic Simulation Group, University of Montana, Missoula, MT, United States of America
[3] Southwest Alaska Network Inventory and Monitoring Program, National Park Service, Anchorage, AK, United States of America
[4] Author to whom any correspondence should be addressed.

E-mail: caleb.pan@mso.umt.edu

Keywords: rain-on-snow, remote sensing, climate change, arctic boreal vulnerability experiment (ABoVE), AMSR, Alaska

Supplementary material for this article is available online

Abstract

Wet snow and the icing events that frequently follow wintertime rain-on-snow (ROS) affect high latitude ecosystems at multiple spatial and temporal scales, including hydrology, carbon cycle, wildlife, and human development. However, the distribution of ROS events and their response to climatic changes are uncertain. In this study, we quantified ROS spatiotemporal variability across Alaska during the cold season (November to March) and clarified the influence of precipitation and temperature variations on these patterns. A satellite-based daily ROS geospatial classification was derived for the region by combining remote sensing information from overlapping MODIS and AMSR sensor records. The ROS record extended over the recent satellite record (water years 2003–2011 and 2013–2016) and was derived at a daily time step and 6 km grid, benefiting from finer (500 m) resolution MODIS snow cover observations and coarser (12.5 km) AMSR microwave brightness temperature-based freeze–thaw retrievals. The classification showed favorable ROS detection accuracy (75%–100%) against *in situ* climate observations across Alaska. Pixel-wise correlation analysis was used to clarify relationships between the ROS patterns and underlying physiography and climatic influences. Our findings indicate that cold season ROS events are most common during autumn and spring months along the maritime Bering Sea coast and boreal interior regions, but are infrequent on the colder arctic North Slope. The frequency and extent of ROS events coincided with warm temperature anomalies ($p < 0.1$), but showed a generally weaker relationship with precipitation. The weaker precipitation relationship was attributed to several factors, including large uncertainty in cold season precipitation measurements, and the important contribution of humidity and turbulent energy transfer in driving snowmelt and icing events independent of rainfall. Our results suggest that as high latitude temperatures increase, wet snow and ROS events will also increase in frequency and extent, particularly in the southwestern and interior regions of Alaska.

1. Introduction

The atmospheric conditions typically associated with high latitude winter rainfall affect the physical properties of the snowpack, including energy content, water content, depth, density and grain size, frequently resulting in a wet snow surface (Singh *et al* 1997). These effects are due to the associated transfers of latent and sensible heat, either directly or through turbulent exchanges that hasten snow melt (Marks *et al* 1998). Whenever snow surface layers reach 0 °C, additional energy flux to the snow surface contributes to melt and rising water content; snowmelt will continue to occur whenever the cold content of the snowpack exceeds 0 °C or until the snow has completely melted (Dingman 2015). Thus, wintertime rain events can be a major driver of wet surface snow conditions indicated from satellite observations (Frei *et al* 2012).

However, rain is not required for wet snow to exist; nor do wet snow conditions always follow rainfall events. Different science communities have used the term 'rain-on-snow' to collectively refer to wet surface snow conditions and the many physical processes that lead to their occurrence. We recognize that rain-on-snow is not necessarily synonymous with wet snow, but that the occurrence of rain on a winter snowpack frequently precedes the presence of wet snow conditions at high latitudes. We therefore retain the usage of the term rain-on-snow (ROS) in this investigation to collectively describe these processes.

Wet snow, and the icing events that frequently follow ROS, affect several ecosystem processes including hydrology, carbon cycling, wildlife movement and human transportation, at multiple spatial and temporal scales (Putkonen and Roe 2003, McCabe *et al* 2007). ROS events, and the positive heat flux to the snowpack often associated with them, are one of the dominant drivers of winter and springtime flooding in mountainous regions and at higher latitudes (Marks *et al* 1998, Guan *et al* 2016, Jeong and Shushama 2018). Enhanced liquid water content (LWC) to the snowpack, whether by ROS or melt events, can also reduce a snowpack's insulating effect on the soil (Lafrenière *et al* 2013, Kim *et al* 2015). Furthermore, accumulated water at the soil surface from ROS-driven snowmelt can release latent heat into the soil horizon, and in turn result in accelerated thawing of frozen ground (Putkonen and Roe 2003, Rennert *et al* 2009). These thawing processes ultimately hasten the release of soil carbon to the watershed and atmosphere in the form of dissolved organic matter or gasses (Hobbie *et al* 2000). Further, accumulated water between the soil surface and snowpack also has the potential to freeze, forming a significant ice barrier to browsing ungulates, which can contribute to large wintertime die-offs (Grenfell and Putkonen 2008, Riseth *et al* 2011, Loe *et al* 2016, Berger *et al* 2018). As intensified warming of the high latitudes, known as 'Arctic Amplification', continues (Serreze and Francis 2006, Cohen *et al* 2014), an increase in the frequency, distribution, and intensity of ROS events is predicted (Jeong and Shushama 2018), with potentially adverse impacts to Arctic ecosystems and the communities that depend on them.

The Arctic Boreal Vulnerability Experiment (ABoVE) is a broad-scale international and interdisciplinary field campaign initiated by NASA to understand environmental change in the Arctic and boreal region (ABR) of western North America and associated linkages to social-ecological systems (Kasischke *et al* 2014). The science objectives of ABoVE include quantifying changes in the condition and distribution of snow, and its impact on ecosystem structure and function. A key limitation to the quantifying and understanding of ROS in the region is a general lack of available observations, which are constrained by its remoteness, severe climate, and sparse regional weather station networks. However, satellite remote sensing methods have been developed for detecting and mapping ROS in the ABR. Successful approaches include the use of active and passive microwave sensors from polar-orbiting satellites that provide frequent observations and enhanced sensitivity to landscape freeze–thaw dynamics (Kimball *et al* 2004, Bartsch 2010b, Semmens *et al* 2013, Wilson *et al* 2013). However, these approaches have generally involved only limited areas and periods, or have relatively coarse (~10–25 km resolution) retrievals.

The objectives of this study were to quantify spatiotemporal variability in ROS across Alaska during the winter season (November–March) and to clarify the influence of precipitation and temperature anomalies on ROS frequency and distribution. The domain for this study is the state of Alaska, which has a long snow season and faces challenges to both natural resources management and socio-economic structure, due to changing snow conditions caused by regional warming trends (Bokhorst *et al* 2016, Kontar *et al* 2018). Much of Alaska is in the ABoVE domain, where a better understanding of the distribution and underlying drivers of ROS will contribute to the ABoVE science objectives and provide critical information to Alaskan land managers.

To address the study objectives, we generated a daily ROS geospatial classification across Alaska by combining synergistic remote sensing information from overlapping MODIS (moderate resolution imaging spectroradiometer) and AMSR (advanced microwave scanning radiometer) sensors. Here, MODIS provides eight-day repeat coverage and relatively fine scale information (500 m resolution) on snow cover extent, while AMSR provides daily microwave brightness temperature (T_b) retrievals sensitive to landscape freeze–thaw dynamics, but within a relatively coarse (~12.5 km) sensor footprint. The combined information from these sensors provides a means for ROS mapping, with enhanced gridding (~6 km resolution) suitable for resolving regional ROS patterns and underlying physiographic and climate drivers.

The application of satellite remote sensing to detect ROS events has progressed in recent years through the development of new data sources and techniques, including both radar (Kimball *et al* 2004, Bartsch 2010b, Bartsch *et al* 2010a), and passive microwave (PM) sensors (Grenfell and Putkonen 2008, Wang *et al* 2013, Wang *et al* 2016). In Alaska, these sensors have been applied to detect ROS using different classification algorithms, including backscatter change detection (Kimball *et al* 2001, Bartsch 2010b, Wilson *et al* 2013), diurnal amplitude variation from PM T_b retrievals (Semmens *et al* 2013), and a T_b differencing approach (Wang *et al* 2016). More recently, spectral gradient ratios, including the Gradient Ratio (GR, Grenfell and Putkonen 2008) and Gradient Ratio Polarization (GRP, Dolant *et al* 2016), were developed to exploit complementary information

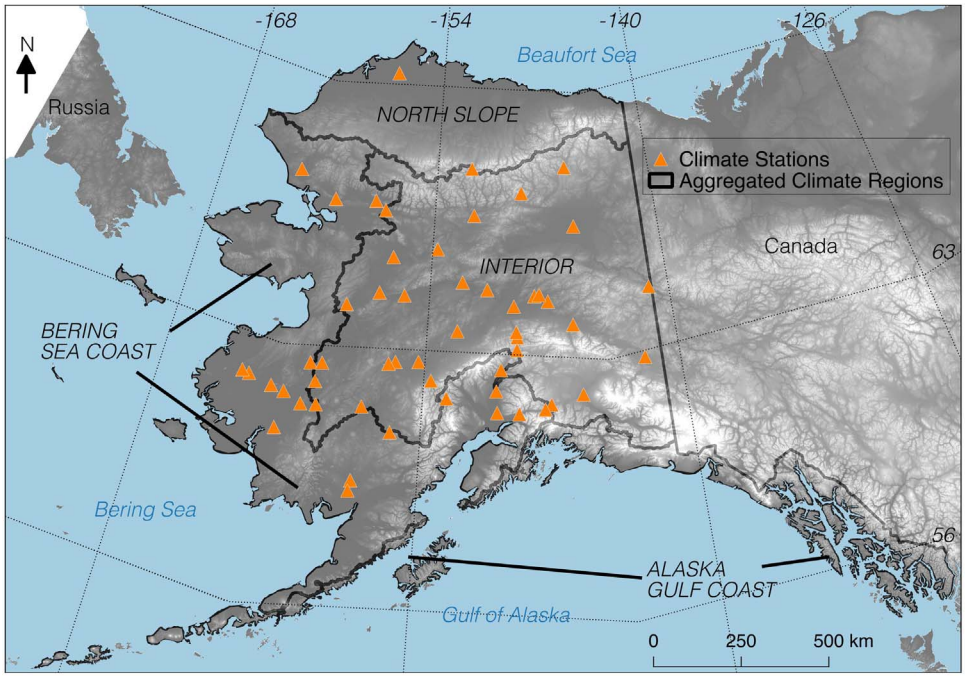

Figure 1. Alaska study domain shown with digital elevation model, climate stations used for tier 2 validation and climate regions used for the ROS correlation analysis.

from different microwave frequencies and polarizations for ROS detection. The PM-based GRP approach was also observed to be effective in detecting ROS and associated winter melt events within the ABR (Dolant *et al* 2016, Langlois *et al* 2017). However, to our knowledge, this study provides the only available ROS satellite record for Alaska that provides 6 km daily resolution from current operational satellites that overlaps with the timing of the ABoVE campaign.

In this study, we used the GRP approach with PM observations from the Advanced Microwave Scanning Radiometer sensors AMSR-E and AMSR2 (hereafter denoted as AMSR) for daily classification of ROS events across Alaska. The AMSR GRP-based ROS classification was conducted over snow-covered areas defined from MODIS. The study period for this investigation encompassed water years (WYs) 2003–2016 and the available AMSR record, which overlapped with the first phase of the ABoVE campaign (Kasischke *et al* 2014). The daily ROS record encompassed the months of November through March, when snowmelt from solar irradiance is minimal and snow cover is widespread and relatively consistent throughout the region (Lindsay *et al* 2015). The ROS classification was mapped to a 6 km resolution grid and used to quantify and understand ROS spatiotemporal variability and underlying drivers across Alaska.

2. Data and methods

2.1. Spatial domain

The state of Alaska spans approximately 20° of latitude and 50° of longitude, encompassing the North Pacific and Arctic Boreal regions of the northern hemisphere. Within the region, many gradients influence the climate, including: latitude, distance from large water bodies, the relative thermal mass and circulation of coastal waters, terrain, and elevation. Alaska is a peninsula with over 10 000 km of coastline, bounded by the Pacific Ocean to the south and the shallower, seasonally ice-covered Bering, Chukchi and Beaufort seas to the west and north. The eastern border of Alaska runs through boreal forest characterized by a cold interior continental climate. Thirteen different climate divisions have been described for the state of Alaska (Bieniek *et al* 2012). For the spatial analysis of ROS distributions, we aggregated the 13 climate divisions into four larger regions delineated by National Hydrography Hydrologic Unit Code (HUC 8) watersheds (USGS 2017) (figure 1). The aggregated Alaska HUC 8 divisions examined for this study include the Alaska Gulf Coast (AGC), Interior (INT), Bering Sea Coast (BSC) and North Slope (NS). These areas reflect Alaska's major climatic regions, of the relatively moderate Pacific maritime, cold-dry boreal interior, and polar arctic northwest coast and North Slope regions. The high latitude ecosystems found in these climate divisions play an important role in the Earth's energy, water and carbon cycles, and are some of the most vulnerable to recent climate warming (Chapin *et al* 2014, O'Neel *et al* 2015).

2.2. Satellite data used for ROS classification

The AMSR-E sensor was launched in 2002 on board the NASA Aqua satellite, and operated until 2011 (Kawanishi *et al* 2003). The AMSR2 follow-on

mission was successfully launched in 2012 on board the JAXA GCOM-W satellite and continues normal operations (Imaoka *et al* 2010, Du *et al* 2014). We used combined calibrated T_b records from AMSR-E for WY 2003–2011 and AMSR2 for WY 2013–2016. The AMSR record was derived using an empirical calibration of similar frequency T_b retrievals from overlapping FY3B Microwave Radiation Imager (MWRI) observations (Du *et al* 2014). The AMSR record has twice-daily, vertical (V) and horizontal (H) polarization T_b retrievals acquired from ascending and descending polar orbital equatorial crossings at 1:30 pm and 1:30 am, which is suitable for detecting ROS (Dolant *et al* 2016, Du *et al* 2016). Lower-frequency T_b retrievals (18.7 GHz and 36.5 GHz, henceforth rounded to 19 and 37 GHz) from the AMSR record were used for ROS detection in this study, as they are sensitive to snow cover properties and landscape freeze–thaw dynamics (Kim *et al* 2017) but insensitive to potential signal degradation from polar darkness, low solar illumination, cloud cover, and atmospheric aerosol contamination effects (Rees *et al* 2010, Tedesco *et al* 2015). The native AMSR T_b footprints are relatively coarse at 19 GHz (27 km × 16 km for AMSR-E and 22 km × 14 km for AMSR2) and at 37 GHz (14 km × 8 km and 12 km × 7 km) due to naturally low PM earth emissions (Kawanishi *et al* 2003, Imaoka *et al* 2010, Frei *et al* 2012). In this study, we used spatially resampled ascending orbit T_b retrievals from the calibrated AMSR record in conjunction with MOD10A2 eight-day maximum snow cover extent (SCE) derived from MODIS (Hall *et al* 2002, Hall and Riggs 2007).

2.3. Spatially resampled AMSR

The AMSR orbital swath T_b data were spatially resampled to a 6 km resolution polar EASE-Grid (version 2) geographic projection, using an inverse distance squared weighting method (Brodzik *et al* 2012, Du *et al* 2017a). To ensure cross-sensor consistency, the gridded AMSR2 T_b data were empirically calibrated against the same AMSR-E frequencies using a double-differencing method and similar overlapping observations from the FY3B MWRI sensor record (Du *et al* 2017b, Du *et al* 2014). The new 6 km grid provided an intermediate resolution between the finer scale (500 m) MODIS SCE and the coarser resolution (~12.5 km) AMSR T_b observations, while enabling enhanced assessment of terrain and land cover spatial heterogeneity.

2.4. Theoretical approach to the ROS classification

We operationally defined ROS days as the satellite PM detection of abrupt changes in surface snow wetness and isothermal states induced by physical processes, such as sensible, latent and turbulent heat exchange that are often associated with winter rainfall. The physical basis of the PM ROS algorithm is the differential response in microwave emissions at 19 (V, H) GHz and 37 (V, H) GHz frequencies to changes in snow cover density and LWC within the snowpack surface. As relatively dry snow initially transitions to wet snow with increasing LWC, T_b increases due to absorption by wet snow (Tedesco *et al* 2015). Yet the interaction between T_b and snow wetness varies over different regions of the microwave spectrum. T_b at 19 (V and H) GHz will change with LWC to a lesser degree than at 37 (V and H) GHz (Rees *et al* 2010, Vuyovich *et al* 2017). Grenfell and Putkonen (2008) found distinct patterns in dielectric properties at 19 and 37 GHz in response to ROS events, leading to their application of a spectral GR that portrays larger differences between V and H polarized (*pol*) T_b retrievals at these frequencies following ROS events equation (1):

$$\mathrm{GR}\left(pol_{(37,19)}\right) = \frac{\left[T_b\,(pol, 37) - T_b\,(pol, 19)\right]}{\left[T_b\,(pol, 37) + T_b\,(pol, 19]\right.}. \quad (1)$$

Dolant *et al* (2016) found that during ROS events, the GR derived from H *pol* T_b (GR-h) returned negative values, while the GR derived from V *pol* T_b (GR-v) returned positive values. This inverse relationship led to the development of the gradient ratio polarization (GRP) between GR-v and GR-h, allowing for the ability to set designated thresholds to classify ROS events. Dolant *et al* (2016) and Langlois *et al* (2017) applied the GRP equation (2) to single-pixel T_b time series from SMMR, SSM/I, and AMSR-E to detect ROS in areas of Quebec and the Canadian Arctic Archipelago.

$$\mathrm{GRP} = \frac{\mathrm{GR} - \mathrm{v}}{\mathrm{GR} - h}. \quad (2)$$

2.5. ROS workflow

In the current study, we applied a similar GRP approach developed from previous studies at point locations (Grenfell and Putkonen 2008, Dolant *et al* 2016, Langlois *et al* 2017) for mapping daily ROS patterns across Alaska. The Alaska regional classification was derived using daily ascending V and H *pol* T_b retrievals at 19 and 37 GHz from the 6 km resolution polar EASE-grid AMSR record. The created workflow is summarized in figure S1 available at stacks.iop.org/ERL/13/075004/mmedia and described below.

We masked water-contaminated pixels induced by the conical scanning of AMSR sensor records (Derksen *et al* 2012, Du *et al* 2016) using a 24 km (~4 pixel) shoreline and water-body buffer created from the 2011, 30 m resolution National Land Cover Database (Homer *et al* 2015). We then used the MODIS SCE record to identify snow-covered areas after screening out low-quality pixels, including missing or degraded snow cover observations, identified by the MOD10A2 product quality flags. The AMSR 37 GHz V *pol* T_b record was analyzed separately, to identify potential snow-covered pixels outside the water body buffer, where $T_b < 265$ K (Vuyovich *et al* 2017). Pixels identified as being snow-covered

Table 1. 2003–2016 observations of ROS events and precipitation totals from Fairbanks, AK (64.80°N, 147.88°W).

Date	Precipitation [mm]
23–26 March 2016	8.89
26 November 2015	< 2.54
21–22 February 2015	5.8
31 December 2014	< 2.54
23–24 January 2014	1.02
5 December 2013	0.51
14–15 November 2013	18.54
14 January 2013	3.81
22–24 November 2010	24.13
2–8 November 2003	11.18
2 March 2003	0.25
8–10 February 2003	7.37

by both the MODIS SCE and AMSR T_b records were then used to derive daily GR and subsequent GRP values for each classified snow pixel over the multi-year (2003–2011, 2013–2016) study period defined by the AMSR record. We applied two different GRP thresholds to classify ROS events for different elevation zones: GRP < 1 was used to identify ROS events below 900 m, while GRP <−5 was used for elevations above 900 m; a more detailed description of the GRP threshold selection is given in the supplementary section (S1). A spatial connectivity threshold of > 10 pixels was then used as a designated size threshold to isolate and analyze more regionally extensive ROS events (Wilson *et al* 2013).

2.6. Two-tiered validation

2.6.1. *Tier 1—empirical in-situ ROS observations*

The Tier-1 validation coupled empirical ROS observations by an observer at the National Weather Service (NWS) field office in Fairbanks, Alaska (table 1), with *in situ* weather station measurements acquired from Fairbanks International Airport (MesoWest ID-PAFA, 134 m above sea level). To determine the agreement between the *in situ* observations and the satellite PM-derived ROS classification, daily mean GRP values were created from 6 km pixels located within a 50 km radius around the Fairbanks station location. Next, the occurrence of the daily mean GRP values < 1 were examined in conjunction with: (1) ROS events empirically observed by the NWS observer; (2) precipitation and fog observations (Wang *et al* 2016) at the station, and; (3) measured precipitation the day before or the day when GRP was < 1.

2.6.2. *Tier 2—climate observation network*

The Tier 2 validation involved an expanded spatial domain employing climate observations across Alaska acquired through the MesoWest and SynopticLabs API (https://synopticlabs.org/api/). The API provided data from several regional weather station networks, including the NWS, remote automated weather stations, and snow telemetry network stations. The climate data were assembled from 235 individual stations to acquire daily surface meteorological parameters, including minimum and maximum air temperatures (T_{min}, T_{max}), average (24-hour) air temperature (T_{avg}), 24-hour accumulated precipitation (prcp), dew point temperature (T_{dew}), and relative humidity (RH). For the study period, 53 of the 235 stations had all of the requested climate variables. The developed Tier 2 workflow is shown in figure S3 and described below.

ROS days classified from the satellite record were validated using *in situ* weather observations from collocated climate stations to identify if rain occurred either the day of or the day before (i−1) a classified ROS event (Obs_{rain}), or if the observed station precipitation was null (Obs_{null}). Given the limitations of wintertime precipitation measurements (Merenti-Valimaki 2001, Martinaitis *et al* 2015, Grossi *et al* 2017), Obs_{null} included conditions where either no precipitation was measured or there was no effective precipitation measurement. Three temperature-driven variables were therefore created and used as a proxy for the rainfall observations (Obs_{rain}), which can have large measurement uncertainty during freeze–thaw transitions (Martinaitis *et al* 2015). The temperature-based Obs_{rain} metrics included wet bulb temperature (T_w), the ratio between daily T_{dew} and T_{avg} (T_{dew}/T_{avg}), and the ratio between daily T_{max} and T_{min} (T_{max}/T_{min}), which were used as indicators for atmospheric moisture and energy flux to surface snow. A more detailed description of the temperature-based precipitation metrics can be found in the supplementary section (S2). We then constrained Obs_{null} by the mean and standard deviations derived from temperature-based Obs_{rain} metrics. ROS days which met all the constraining conditions set by Obs_{rain} were classified as commission, whereas all Obs_{null} observations that did not meet the defined conditions were classified as omission.

2.7. *Statistical methods and climate anomalies*

Due to the relatively short study period and a data gap between the AMSR-E and AMSR2 records in 2012, we did not attempt to perform a temporal trend analysis of the ROS results. However, we did calculate the mean, standard deviation and coefficient of variation (C_v) of monthly total ROS days. The C_v was used to characterize the relative dispersion of ROS days (Sugg *et al* 2017), with higher values equating to high variability and low predictability, with the inverse being true as the C_v approaches zero (Frei *et al* 2012).

Pixel-wise correlations were performed to determine the sign and strength of relationships between monthly total ROS days and respective climate anomalies. Climate anomalies were derived using 1 km resolution gridded daily surface weather station observations from the North America Daymet record (Thornton *et al* 1997). Daymet was one of the few products available for Alaska with a spatial (1 km^2) and temporal resolution similar to the AMSR-derived ROS record. Daymet daily T_{min}, T_{max}, and prcp for the period from 1980 to 2016 were acquired from the DOE ORNL data portal

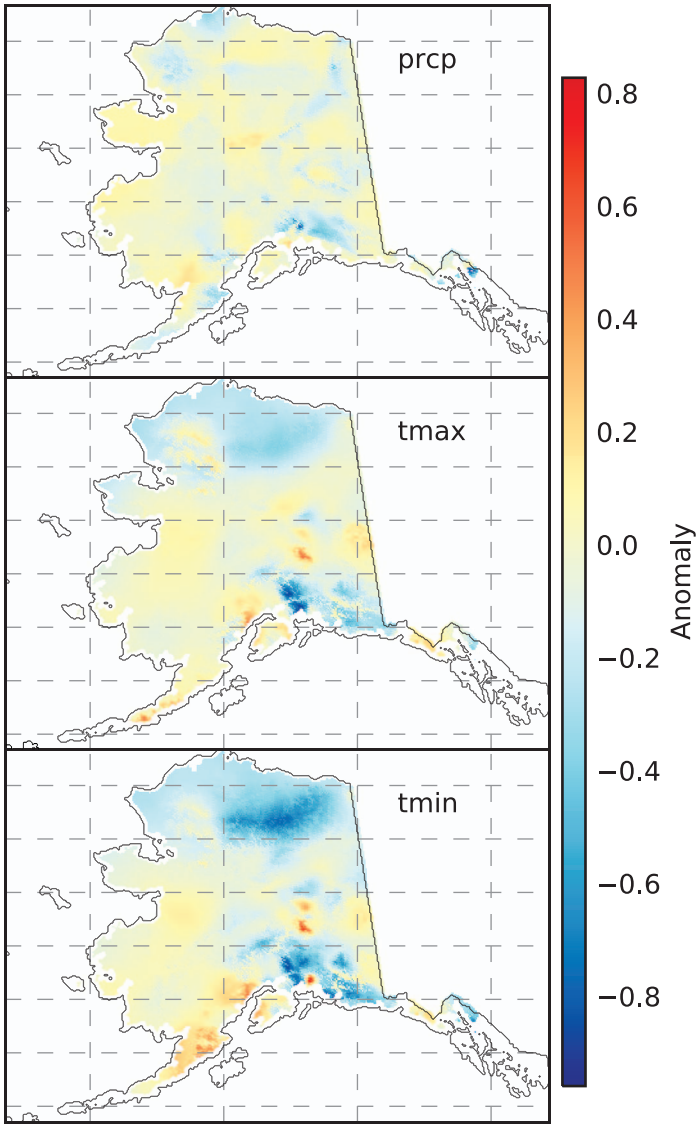

Figure 2. Daymet-derived standardized anomalies for prcp (top), T_{min} (middle), and T_{max} (bottom) from 2003 to 2016 (excluding 2012) over the Alaska study domain; a 24 km coastal mask (white areas) is used to minimize open water body effects on the PM retrievals.

(www.daymet.ornl.gov/dataaccess.html). The 1 km Daymet data were resampled to the 6 km study grid and used to create a baseline monthly mean climatology and standard deviation for each pixel and climate parameter. Here, the baseline climatology was assembled from a 23-year Daymet historical record (1980–2002). Monthly mean annual values of each climate parameter were then derived for each year of record from 2003 to 2016 (excluding 2012) and used with the respective climatology for each pixel to create gridded normalized anomalies (figure 2).

3. Results

3.1. Tier-1 validation

The Tier 1 validation indicated strong agreement between PM-observed ROS and the occurrence of liquid precipitation from both direct measurements and empirical observations. Of the three types of precipitation validation measurements and observations, no single type showed consistent agreement with the PM-observed ROS record (table 2). Of the 11 ROS event observations made by the NWS observer over the 13-year record, ten were detected as PM-observed ROS days. The precipitation type observations (rain, fog) from the PAFA station provided more overall observations than the direct precipitation measurements, but were unable to identify all ROS events consistently (figures 3(*a*) and (*b*)). Yet, for the years of interest, ROS omission errors indicated from all three types of validation observations ranged from 0 to 5 events, with associated accuracies ranging from 75% to 100%.

The results summarized in figures 3(*a*) and (*b*) also show several days in early November when the GRP was < 1, suggesting early wintertime freeze–thaw transitions due to sensible and latent heat flux, as

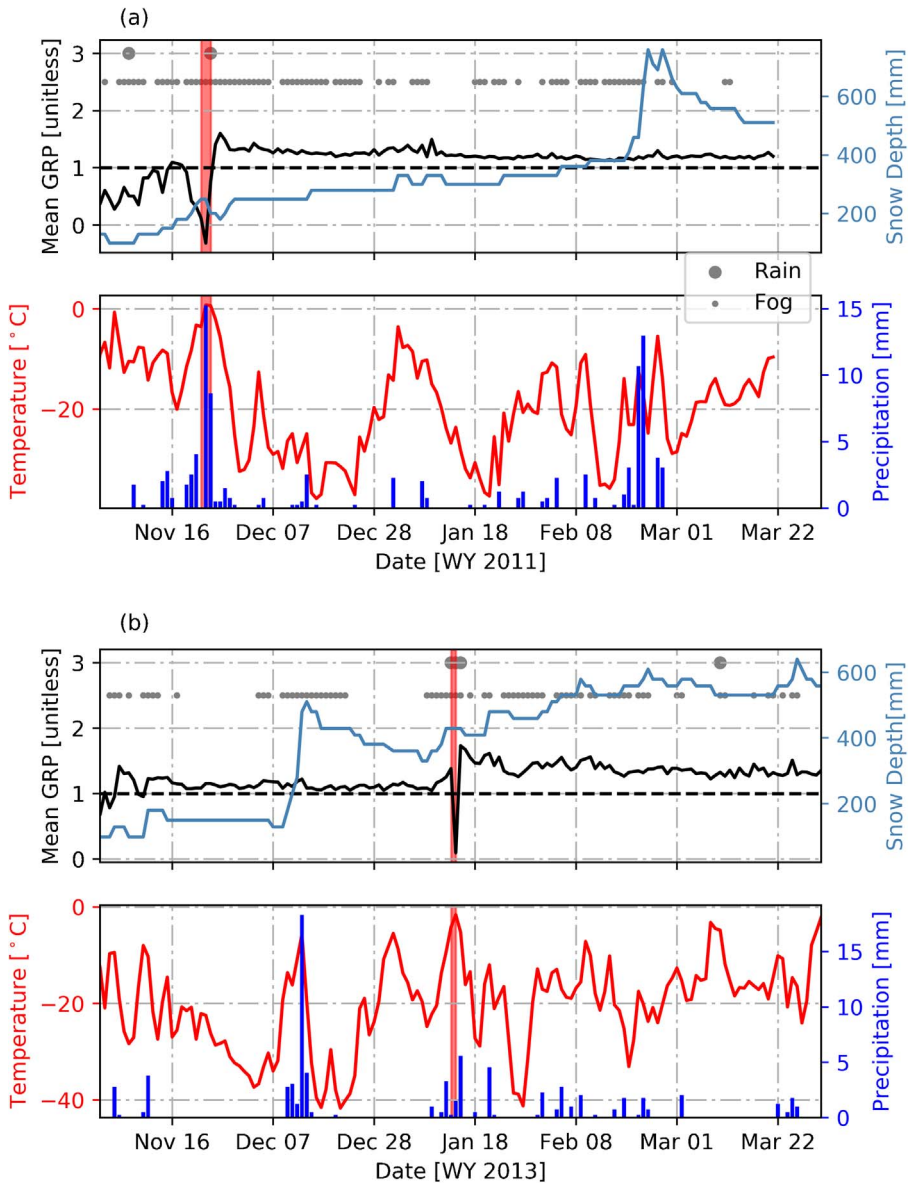

Figure 3. (*a*) and (*b*) PM-derived daily mean GRP values and *in situ* precipitation, temperature, snow depth, rain and fog observations from Fairbanks, Alaska for 2011 and 2013 water years; red vertical bars indicate NWS-observed ROS events and dashed black horizontal line indicates the GRP threshold.

Table 2. Tier-1 validation of PM-observed ROS omissions and accuracy.

WY	NWS empirical[a]	PAFA prcp type[b]	PAFA measured prcp[c]	Total ROS events	Accuracy %	+/− error ROS events
2003	3/3	9	6	15	100.00	0
2004	1/1	9	0	9	100.00	0
2011	1/1	17	14	22	95.45	1
2013	1/1	5	7	8	75.00	2
2014	1/1	35	38	46	89.13	5
2015	1/2	6	1	22	100.00	0
2016	2/2	15	15	16	93.75	1

[a] PM-detected ROS days/empirical ROS observations made by NWS observer.

[b] Precipitation observed at PAFA, includes rain and fog.

[c] Measured precipitation at PAFA on the day of, or the day before, a detected ROS event.

there was limited precipitation measured during this period. Also, significant snowfall is reported in late February (figure 3(*a*)) and early December (figure 3(*b*)). During these snowfall events, the GRP remained above the detection threshold, which suggested confidence in the identification of ROS rather than snowfall events when GRP was < 1 and measured precipitation was > 0.

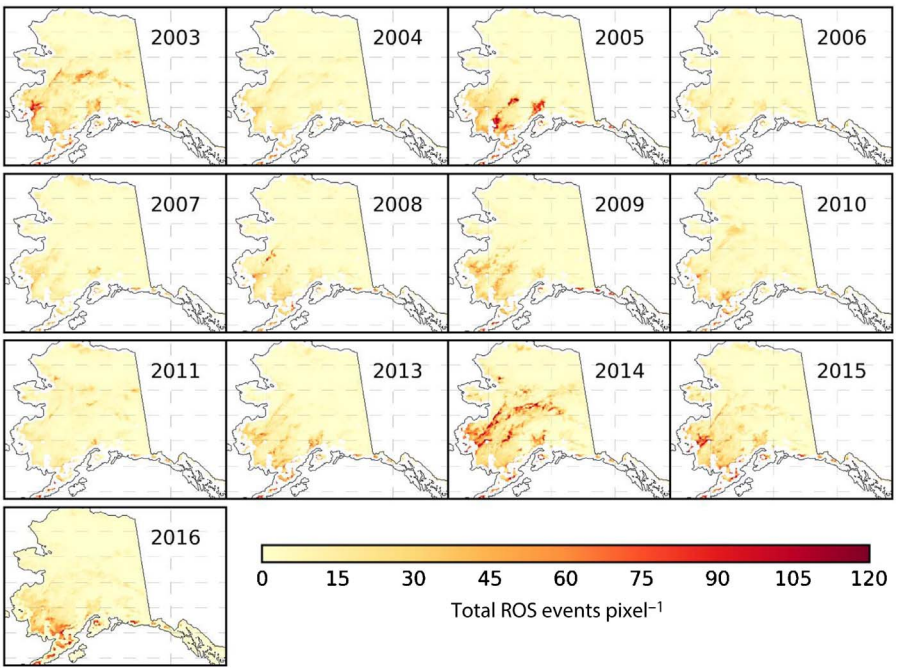

Figure 4. Time series of annual days with ROS summed for each pixel, with 24 km coastal mask used to minimize open water body effects on the PM retrievals.

Table 3. Tier-2 validation of PM observed ROS days.

	November–March
Obs_{rain}	54
Obs_{null}	224
Commission	183
Omission	41
Total ROS Events	278
Accuracy [%]	85.9
+/− Error [ROS Events]	39

3.2. Tier-2 validation

During the study period, 278 PM-detected ROS events occurred at the 53 Alaska climate station locations. Of these 278 events, 54 coincided with *in situ* station precipitation measurements either the day of or the day before the PM-detected ROS event (Obs_{rain}). The remaining 224 PM days with ROS coincided with *null* precipitation observations (Obs_{null}). After the constraining process, 41 Obs_{null} observations were classed as errors of omission, while the remaining 183 Obs_{null} observations were classed as errors of commission. The combined commission errors with Obs_{rain} produced a final PM ROS classification accuracy of 86% (table 3). Further discussion on the limitations and caveats of validating the PM-derived ROS events is presented in the supplement (S4).

3.3. Temporal and spatial patterns of ROS

For the entire study period, about 52% of Alaska was affected by at least one ROS day on average; however, the ROS distribution showed large temporal variability (figure 4). For example, in WY 2005 about 38% of the domain experienced a ROS event, compared to a maximum of 72% in WY 2014. With respect to frequency, during the study period about 27% of the domain experienced at least five ROS days in a given year; this percentage peaked at 51% in WY 2014 and dropped to 16% in WY 2006. Some years of record showed relatively frequent and widespread ROS occurrences (WYs 2003, 2005, and 2014), while other years had far fewer ROS events (e.g. WYs 2004, 2006, and 2011). A visual comparison between our annual results and Wilson *et al* (2013) showed good agreement, particularly for WYs 2003 and 2005. However, results must be seen as a relative comparison as Wilson *et al* (2013) included October and April in their annual summations. Both studies indicated a higher occurrence of freeze–rethaw or ROS days in the southwestern portion of Alaska. Bartsch (2010b) also detected melt events across Alaska using daily 13.4 GHz (Ku-band) radar backscatter retrievals from QuickSCAT during the same period and as Wilson *et al* (2013) and found similar results. But more interestingly, PM-derived melt events (Semmens *et al* 2013, Wang *et al* 2016) and active microwave melt events (Bartsch 2010b, Wilson *et al* 2013) demonstrated similar results to this study, an increasing trend in events moving from the central interior region and into southwest Alaska.

The PM-observed ROS days showed the greatest occurrence in the southwest and central portions of Alaska, including the BSC, AGC, and INT regions, but the frequency and intensity of these events showed large year-to-year variability. The temporal variation by WY and month in PM-detected ROS days for each Alaskan sub-region is shown in figure 5; these results indicate that the BSC and north central portions of the AGC consistently possessed the highest mean

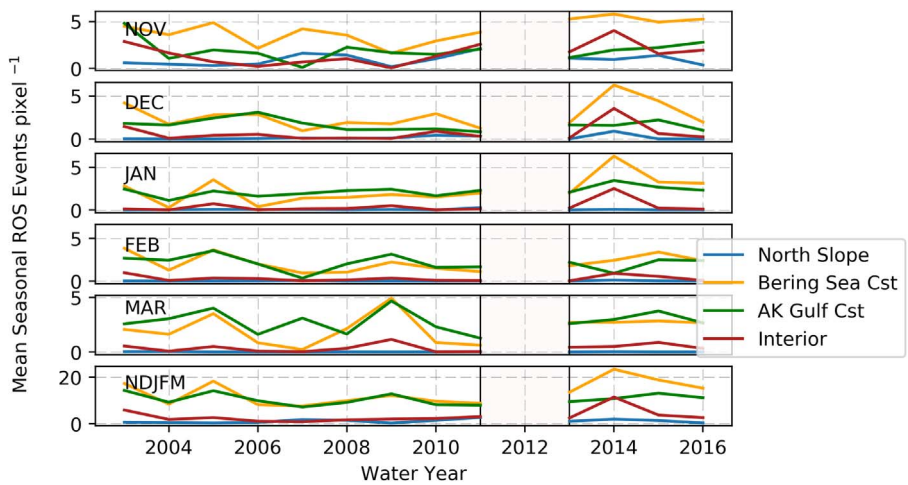

Figure 5. Time series of mean ROS days per pixel and per WY for aggregated Alaskan climate regions from WYs 2003–2016.

Table 4. Monthly ROS statistics by climate region.

	North slope (NS)			Bering sea coast (BSC)			AK Gulf coast (AGC)			Interior (INT)		
	mean	sd	Cv	mean	sd	Cv	mean	sd	Cv	mean	sd	Cv
November	0.91	0.71	0.91	4.04	2.07	0.49	1.93	0.92	0.42	1.56	1.19	0.66
December	0.15	0.15	1.00	2.67	1.30	0.58	1.63	0.66	0.51	0.65	0.49	0.82
January	0.04	0.04	NA	2.29	1.81	0.63	2.19	0.50	0.30	0.37	0.34	0.95
February	0.02	0.02	NA	2.12	1.79	0.78	2.11	0.61	0.35	0.29	0.28	0.96
March	0.01	0.01	NA	2.14	1.52	0.63	2.79	0.87	0.32	0.38	0.40	0.87

number of annual ROS days [pixel^{-1}]. Except for WY 2003 and WY 2014, the INT and NS regions experienced ROS almost exclusively in the month of November.

An inter-annual comparison between the freeze–rethaw record of Wilson *et al* (2013) derived from QuickSCAT and our calculated ROS events showed strong agreement from November to March (2003–2008). Both studies indicated that the largest spatial coverage of such events occurred in November, while the NS experienced no events during March in either study. Wilson *et al* (2013) reported that the NS did not experience any form of melt events until April. The results of the analysis of melt events of Wang *et al* (2016) from 25 km PM retrievals also supported the temporal and geographical pattern in the NS. Summary statistics in table 4 show that the C_v during November and December in the NS is quite high at 0.91 and 1, respectively. These values indicate that even during November and December, ROS days are still an uncommon event across the NS.

3.4. Correspondence between ROS events, temperature, and precipitation

Linear regressions between temperature departure data, provided by the Alaska Climate Data Center (figure S4), and the PM-derived mean seasonal ROS events indicated that temperature had the greatest explanatory power for predicting ROS events within the BSC ($p < 0.001$) followed by the INT ($p < 0.01$) and AGC ($p < 0.01$) regions (figure 6). In the NS, the temperature departure was insensitive to ROS occurrence ($p < 0.9$), likely due to colder climate conditions and a lower overall number of ROS events detected in the region. However, ROS events are sensitive not just to temperature, but rather the interactions between temperature, humidity, and precipitation. A correlation analysis between PM-derived ROS and Daymet-derived climate anomalies aided in exploring these interactions.

The correlations between monthly (November–March) climate anomalies and days with ROS were statistically significant ($p \leq 0.1$) in many locations (figure 7). Overall, days with ROS coincided with above-normal precipitation and temperature, with notable temporal and spatial variability in both the sign and strength of the relationships. The relationships between days with ROS and temperature, and precipitation showed greater spatial heterogeneity in November than in December, as both positive and negative relationships are observed. However, from January through March, ROS days and climate anomaly correlations became positive, with the strongest of these positive correlations occurring in February. Correlation patterns were similar for both daily minimum and maximum air temperatures and ROS events over all months represented.

Aggregated correlations for ROS days and associated climate anomalies by Alaska climate regions showed consistently positive correlations from January through March for all regions except the NS

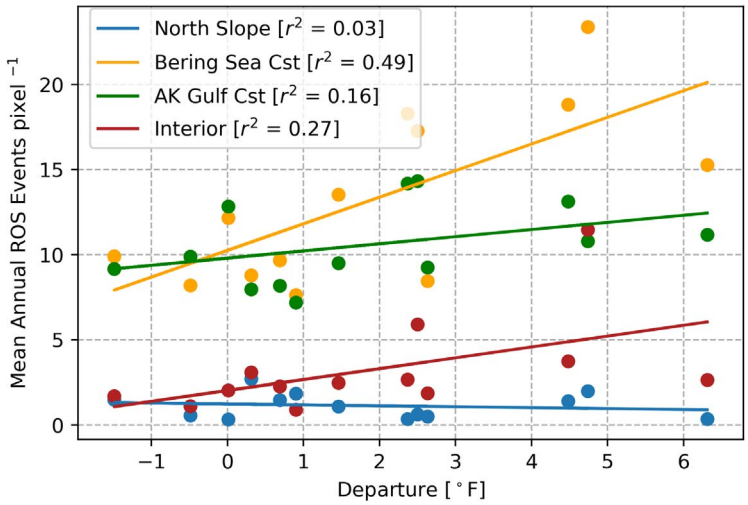

Figure 6. Relationship between mean annual (WY) days with ROS per pixel and surface air temperature departures (°F) aggregated within each Alaska climate region for each year of record from 2003 to 2016.

(figure 8). In November and December, the mean temperature correlations remained positive but had a large spread in the correlation distribution, including both positive and negative relationships. The mean precipitation correlations in November and December were negative in the BSC and INT regions, but as with temperature, also showed a large range of variability. The negative correlations may be a consequence of the uncertainty introduced by the Daymet model (Daly *et al* 2008, Oyler *et al* 2015), but could also be a consequence of using a maximum snow cover extent product (MOD10A2) during periods of intermittent snow. The NS region showed a predominantly positive relationship with temperature, but a more variable relationship with minimum temperature in March. Precipitation correlations in the NS were sporadic and weak due to the characteristic colder and drier Arctic climate of the region, which showed a paucity of PM-derived ROS events during the December–March period, when seasonal temperatures are generally well below freezing and the cold Arctic air mass holds little moisture. Also shown in figure 2 are below normal temperature anomalies across the NS during the study period, which also likely contributed to the infrequent occurrence of ROS days across the region.

4. Discussion

4.1. Sources of error, limitations, and advances

The PM ROS events over Alaska showed variable correlations with the selected climate anomalies during November and December, particularly in regions with low elevation (< 200 m) pixels. Inconsistent correlations may also indicate the occurrence of misclassified pixels at lower elevations. The combination of the high variability in correlations and greater occurrence of PM-derived ROS events indicates that these areas are influenced by wet snow and by shallow, transient snowpack conditions frequently found in low-elevation landscapes (Rees *et al* 2010). The high-density network of tundra lakes at low elevations in the BSC region, in addition to large proglacial lakes in southwest Alaska, may also contribute to the higher number of PM-derived ROS observations in the region (Wilson *et al* 2013, Wang *et al* 2016). The generally greater occurrence of freeze–thaw events in early November and late March in these regions may contribute additional uncertainty, such that the ROS algorithm may be detecting increased LWC introduced by snowmelt in the absence of rainfall or atmospheric condensation (Dolant *et al* 2016).

Our validation results from Fairbanks, AK, showed that most ROS events occurred in early November. The timing of ROS events coincided with many fog observations, indicating that latent and turbulent heat flux driven snowmelt may have contributed to the ROS detection during periods with no measured precipitation (Semmens *et al* 2013, Wang *et al* 2016). These results are also consistent with a prior study indicating that fog and positive temperatures are a primary driver of melt events in the Yukon River Basin (YRB), and that that the presence of fog is an effective indicator for warm air intrusions (Semmens *et al* 2013).

The results from this study were similar to the ROS spatial and seasonal patterns reported from previous studies involving different satellite microwave sensors, classification algorithms and study periods (Bartsch 2010b, Semmens *et al* 2013, Wilson *et al* 2013 and Wang *et al* 2016). These similar findings include a generally greater occurrence of melt events in the southwestern part of Alaska. The studies show that melt events are very infrequent from November to March, but increase dramatically further into spring. While the combined results from these studies indicated multiple effective methods for classifying and documenting ROS and associated melt events from different

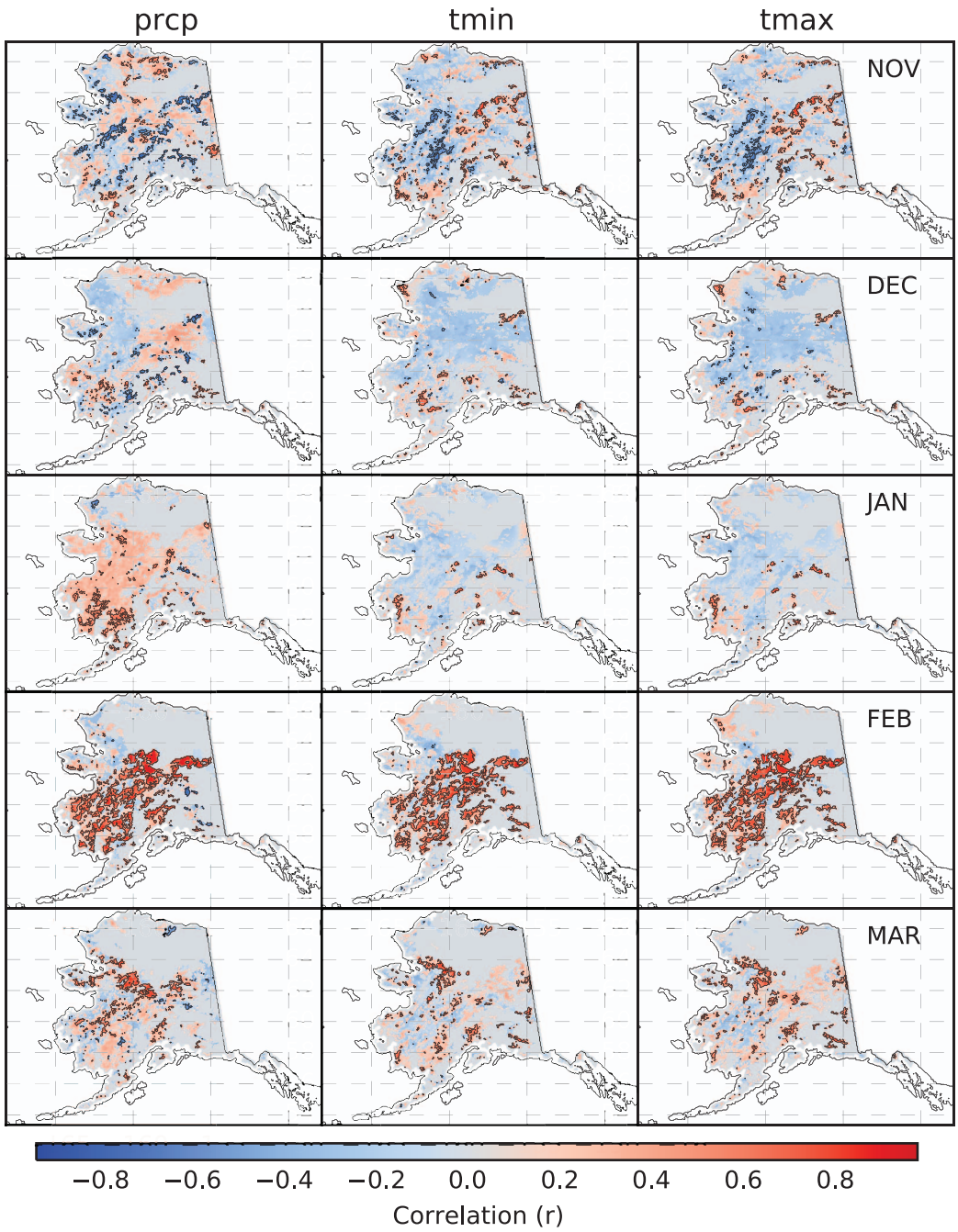

Figure 7. Daymet-derived climate anomalies and ROS correlations from November to March in Alaska from 2003 to 2016 (2012 excluded); black contour lines indicate pixels with > 90% confidence level.

algorithms and sensors, they do not utilize ongoing sensor missions and/or report ROS events at a 6 km resolution. In this study we address this by: (1) creating a new ROS record over Alaska using synergistic MODIS and AMSR-E/2 observations that overlap the NASA ABoVE campaign, while enabling continuity of the ROS record through continuing satellite operations; (2) using an algorithm approach that requires only limited inputs emphasizing MODIS SCE and AMSR T_b retrievals, while the combined information from these sensors supported finer (6 km) resolution delineations of ROS patterns and environmental gradients; (3) providing a regional application of the GRP algorithm, which extended previous localized GRP applications involving *in situ* field sites (Grenfell and Putkonen 2008, Dolant *et al* 2016, Langlois *et al* 2017).

Future ROS record versions will continue to focus on refining the GRP threshold to more effectively account for variations in snow conditions and constraining uncertainties over different land cover types. Yet, regardless of the threshold challenges, this study demonstrated the utility and effectiveness in using the GRP to detect ROS and associated melt events across a large boreal-Arctic landscape. Potential applications of the GRP to detect other snow processes including snow onset, melt onset, and duration remain to be explored.

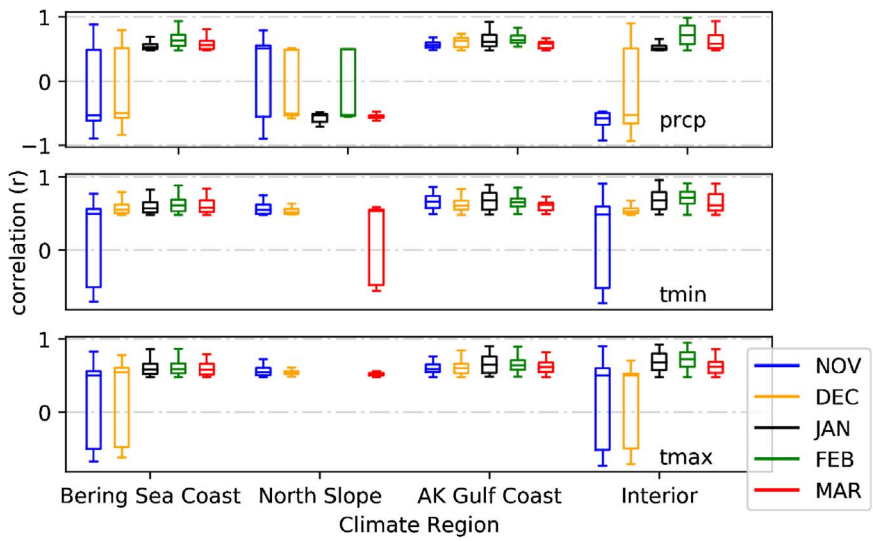

Figure 8. Boxplot summaries for climate anomaly and ROS day correlations for all pixels where $p \leq 0.1$, aggregated by Alaska climate region for each month (November–March) from 2003 to 2016 (excluding 2012).

4.2. Consequences of climate change and ROS events in Alaska

Studies examining projected temperature and precipitation trends over Alaska in the latter part of the 21st century indicated future warmer winter and annual temperature conditions across the state (Stafford *et al* 2000, Serreze and Francis 2006, Bieniek *et al* 2014); and historically, over the past 60 years, Alaska has experienced almost double the rate of warming relative to other regions in the United States (Chapin *et al* 2014). While our results from both temperature departures and climate anomalies indicated that ROS frequency is intensified in years with anomalously high temperatures, these temperature anomalies are often driven by large-scale atmospheric circulation patterns that have been found to be highly correlated with ROS (Cohen *et al* 2015). Such warm events in Alaska are associated with southwesterly flows and Pacific-North American (PNA) pressure systems that promote ROS and melt events from October to December (Rennert *et al* 2009, Semmens *et al* 2013). More recent studies indicated that stratospheric circulations (i.e. polar vortex) strongly influence Alaskan winter temperatures. Specifically, during periods of a weak polar vortex, cold polar air masses are replaced by warmer conditions known as 'warm Arctic cold continents' (Overland and Wang 2010, Cohen *et al* 2014, Kretschmer *et al* 2018), which may promote ROS and associated melt events. The atmospheric blocking and enhanced winter temperatures are also purported to be a major driver of recent record warm Arctic temperatures and record low sea ice extents (Cohen 2016).

Projected warming trends across Alaska and the Arctic (Chapin *et al* 2005) are expected to increase variability in regional snow cover conditions. Model simulations projected a 10%–20% decrease in SCE across the Arctic by 2050, with the greatest losses over Alaska (Callaghan *et al* 2011). These warming trends may also increase the frequency, duration and extent of surface thawing and refreezing, rainfall and mixed precipitation events, altering snowpack structure and decreasing snow-covered area and duration (Chapin *et al* 2005, Callaghan *et al* 2011, Cohen *et al* 2015, Kim *et al* 2015). All these factors are expected to contribute to the polar amplification of global warming due to the important role of snow cover on surface albedo and the terrestrial energy budget (Serreze and Francis 2006, Derksen and Brown 2012). The changing snow cover conditions are also expected to impact regional hydrology and ecosystem processes, due to the role of snow cover as an important water storage and thermal buffer influencing underlying soil active layer temperature and moisture constraints on ecosystem processes, and permafrost stability (Cohen *et al* 2012, Yi *et al* 2015). Some studies suggested that ROS events will become more common in a warming climate across the ABR (Semmens *et al* 2013, Jeong and Shushama 2018), which is consistent with an analysis of the recent historical record reporting an annual increase of about seven melt event days per year from 1998 to 2013 over the pan-Arctic (Wang *et al* 2016). However, the long-term influence of enhanced ROS and melt events within Alaska and the associated impacts of these changes on the regional hydrology, ecosystems and human populations remain uncertain.

5. Summary

This paper presented a new satellite-derived ROS dataset derived from MODIS snow cover observations and a passive microwave spectral gradient

ratio-based classification (Dolant *et al* 2016) derived using calibrated 6 km AMSR T_b records at 19 GHz and 37 GHz frequencies. The daily ROS classification was conducted over Alaska for the winter months (November–March) from WYs 2003–2016 (excluding 2012). A two-tiered validation approach using regional weather station observations indicated favorable ROS classification accuracies ranging from 75% to 100%. The resulting multi-year satellite record revealed markedly higher ROS frequencies in the southwest and central portions of Alaska. The ROS days also occurred most frequently in November and December and coincided with warm temperature anomalies. ROS events were consistently observed in the BSC and AGC during all months of the year, and often occurred during periods of above-normal temperatures in the INT and NS regions. These results were similar to previous remote sensing-based ROS studies derived over different periods and using different classification algorithms; together, these results indicate strong sensitivity of satellite microwave remote sensing to related ROS processes.

The northern boreal and Arctic regions are characterized by an extended period of seasonal snow cover, which strongly influence regional ecosystems, hydrological processes, the surface energy budget and global climate. As the northern latitudes continue to experience accelerated warming at roughly twice the mean global rate, ROS is expected to play a more significant role in both ecological and hydrological processes. To understand future implications of enhanced ROS events, we presented a ROS algorithm that utilized satellite observations from current operational satellites (AMSR2, MODIS), enabling ROS retrievals over Alaska that overlap with recent extensive and planned field campaigns from the NASA ABoVE. Thus, the data record developed in this study, when synthesized with other biophysical observations, are expected to contribute to addressing several data gaps and ABoVE science objectives pertaining to climate-related impacts on boreal and Arctic ecosystems, wildlife, permafrost hydrology and snow processes, and associated climate impacts on human-natural systems.

Acknowledgments

We thank Rick Thoman and the Fairbanks NWS staff for their contributions of validation data, and the Alaska Climate Research Center for their temperature departure contributions. We also thank Nathaniel Robinson for helpful comments on an earlier version of this manuscript along with three anonymous reviewers for their constructive comments that greatly improved this paper. This research was funded by the National Park Service Southwest Alaska Network and the NASA Arctic Boreal Vulnerability Experiment (ABoVE) (NNX15AT74A). The ROS record are publicly archived at the Oak Ridge National Laboratory (ORNL) through the Distributed Active Archive System (DAAC) and through the following link http://files.ntsg.umt.edu/data/AMSR_ROS/.

ORCID iDs

Caleb G Pan https://orcid.org/0000-0002-4510-2022
Peter B Kirchner https://orcid.org/0000-0001-9770-5530
John S Kimball https://orcid.org/0000-0002-5493-5878
Youngwook Kim https://orcid.org/0000-0003-0697-2575
Jinyang Du https://orcid.org/0000-0002-8698-6696

References

Bartsch A, Kumpula T, Forbes B C and Stammler F 2010a Detection of snow surface thawing and refreezing in the Eurasian Arctic with QuickSCAT: implications for reindeer herding *Ecol. Appl.* **20** 2346–58

Bartsch A 2010b Ten years of SeaWinds on QuickSCAT for snow applications *Remote Sens.* **2** 1142–56

Berger J, Hartway C, Gruzdev A and Johnson M 2018 Climate degradation and extreme icing events constrain life in cold-adapted mammals *Sci. Rep.* **8** 1156

Bieniek P A *et al* 2012 Climate divisions for Alaska based on objective methods *J. Appl. Meteorol. Climatol.* **51** 1276–89

Bieniek P A, Walsh J E, Thoman R L and Bhatt U S 2014 Using climate divisions to analyze variations and trends in Alaska temperature and precipitation *J. Clim.* **27** 2800–18

Bokhorst S *et al* 2016 Changing Arctic snow cover: a review of recent developments and assessment of future needs for observations, modelling, and impacts *AMBIO* **45** 516–37

Brodzik M J, Billingsley B, Haran T, Raup B and Savoie M H 2012 EASE-Grid 2.0: incremental but significant improvements for Earth-gridded data sets *ISPRS Int. J. Geo.-Inf.* **1** 32–45

Callaghan T V *et al* 2011 The changing face of arctic snow cover: a synthesis of observed and projected changes *AMBIO* **40** 17–31

Chapin III F S, Trainor S F, Cochran P, Huntington H, Markon C, McCammon M, McGuire A D and Serreze M 2014 *Climate Change Impacts in the United States: The Third National Climate Assessment* ed J M Melillo, T C Richmond and G W Yohe (Washington, DC: US Global Change Research Program) pp 514–36

Chapin III F S *et al* 2005 Role of land-surface changes in Arctic summer warming *Science* **310** 657–60

Cohen J, Furtado J C, Barlow M A, Alexeev V A and Cherry J E 2012 Arctic warming, increasing snow cover and widespread boreal winter cooling *Env. Res. Lett.* **7** 014007

Cohen J *et al* 2014 Recent Arctic amplification and extreme mid-latitude weather *Nat. Geo.* **7** 627–37

Cohen J, Ye H and Jones J 2015 Trends and variability in rain-on-snow events *Geophys. Res. Lett.* **42** 1–8

Cohen J 2016 An observational analysis: tropical relative to Arctic influence on mid-latitude weather in the era of Arctic amplification *Geophys. Res. Lett.* **43** 5287–94

Daly C, Halbleib M, Smith J I, Gibson W P, Doggett M K, Taylor G H and Pasteris P P 2008 Physiographically sensitive mapping of climatological temperature and precipitation across the conterminous United States *Int. J. Clim.* **28** 2031–64

Derksen C and Brown R 2012 Spring snow cover extent reductions in the 2008–2012 period exceeding climate model projections *Geophys. Res. Lett.* **39** 1–6

Derksen C, Toose P, Lemmetyinen J, Pulliainen J, Langlois A, Rutter N and Fuller M C 2012 Remote sensing of environment evaluation of passive microwave brightness temperature simulations and snow water equivalent retrievals through a winter season *Remote Sens. Environ.* **117** 236–48

Dingman S L 2015 *Physical Hydrology* 3rd edn (Long Grove, IL: Waveland Press) p 643

Dolant C, Langlois A, Montpetit B, Brucker L, Roy A and Royer A 2016 Development of a rain-on-snow detection algorithm using passive microwave radiometry *Hydrol. Process.* **30** 3184–96

Du J, Kimball J S, Duguay C, Kim Y and Watts J D 2017 Satellite microwave assessment of Northern Hemisphere lake ice phenology from 2002–2015 *Cryosphere* **11** 47–63

Du J, Kimball J S, Jones L A, Kim Y, Glassy J and Watts J D 2017b A global satellite environmental data record derived from AMSR-E and AMSR2 microwave Earth observations *Earth Syst. Sci. Data* **9** 791–808

Du J, Kimball J S, Shi J, Jones L A, Wu S, Sun R and Yang H 2014 Inter-calibration of satellite passive microwave land observations from AMSR-E and AMSR2 using overlapping FY3B-MWRI sensor measurements *Remote Sens.* **6** 8594–616

Frei A, Tedesco M, Lee S, Foster J, Hall D K, Kelly R and Robinson D A 2012 A review of global satellite-derived snow products *Adv. Sp. Res.* **50** 1007–29

Grenfell T C and Putkonen J 2008 A method for the detection of the severe rain-on-snow event on Banks Island, October 2003, using passive microwave remote sensing *Water Resour. Res.* **44** 1–9

Grossi G, Lendvai A, Peretti G and Ranzi R 2017 Snow precipitation measured by gauges: systematic error estimation and data series correction in the Central Italian Alps *Water* **9** 1–14

Guan B, Waliser D E, Ralph F M, Fetzer E J and Neiman P J 2016 Hydrometeorological characteristics of rain-on-snow events associated with atmospheric rivers *Geophys. Res. Lett.* **43** 2964–73

Hall D K, Riggs G A, Salomonson V V, DiGirolamo N E and Bayr K J 2002 MODIS snow-cover products *Remote Sens. Environ.* **83** 181–94

Hall D and Riggs G 2007 Accuracy assessment of the MODIS snow products *Hydrol. Process.* **21** 1534–47

Hobbie S E, Schimel J P, Trumbore S E and Randerson J R 2000 Control over carbon storage and turnover in high-latitude soils *Glob. Change Biol.* **6** 196–210

Homer C G, Dewitz J A, Yang L, Jin S, Danielson P, Xian G, Coulston J, Herold N D, Wickham J D and Megown K 2015 Completion of the 2011 national land cover database for the conterminous United States—representing a decade of land cover change information *Photogramm. Eng. Remote Sens.* **81** 345–54

Imaoka K, Kachi M, Kasahara M, Ito N, Nakagawa K and Oki T 2010 Instrument performance and calibration of AMSR-E and AMSR2 *Int. Arch. Photogramm. Remote Sens. Spat. Inf. Sci. ISPRS Arch.* **38** 13–8

Jeong D and Sushama L 2018 Rain-on-snow events over North America based on two Canadian regional climate models *Clim. Dyn.* **50** 303–16

Kasischke E S *et al* 2014 A concise experiment plan for the Arctic-boreal vulnerability experiment *Natl Aero. Spc. Admin.* 1–108

Kawanishi T, Sezai T, Ito Y, Imaoka K, Takeshima T, Ishido Y, Shibata A, Miura M, Inahata H and Spencer R W 2003 The advanced microwave scanning radiometer for the Earth observing system (AMSR-E), NASDA's contribution to the EOS for global energy and water cycle studies *IEEE Trans. Geosci. Remote Sens.* **41** 184–93

Kim Y, Kimball J S, Glassy J and Du J 2017 An extended global Earth system data record on daily landscape freeze—thaw status determined from satellite passive microwave remote sensing *Earch Syst. Sci. Data* **9** 133–47

Kim Y, Kimball J S, Robinson D A and Derksen C 2015 New satellite climate data records indicate strong coupling between recent frozen season changes and snow cover over high northern latitudes *Environ. Res. Lett.* **10** 1–10

Kimball J S, McDonald K C, Keyser A R, Frolking S and Running S W 2001 Application of the NASA Scatterometer (NSCAT) for determining the daily frozen and nonfrozen landscape of Alaska *Remote Sens. Environ.* **75** 113–26

Kimball J S, McDonald K C, Frolking S and Running S W 2004 Radar remote sensing of the spring thaw transition across a boreal landscape *Remote Sens. Environ.* **89** 163–75

Kontar Y Y, Eichelberger J C, Gavrilyeva T N, Filippova V V, Savvinova A N, Tananaev N I and Trainor S F 2018 Springtime flood risk reduction in rural Arctic: a comparative study of interior Alaska, United States and Central Yakutia, Russia *Geosciences* **8** 1–21

Kretschmer M, Coumou D, Agel L, Barlow M, Tziperman E and Cohen J 2018 More-persistent weak stratospheric polar vortext states linked to cold extremes *Bull. Am. Meteorol. Soc.* **January** 49–60

Lafrenière M J, Laurin E and Lamoureux S F 2013 The impact of snow accumulation on the active layer thermal regime in high Arctic soils *Vadose Zone J.* **12** 1–13

Langlois A *et al* 2017 Detection of rain-on-snow (ROS) events and ice layer formation using passive microwave radiometry: a context for Peary caribou habitat in the Canadian Arctic *Remote Sens Environ.* **189** 84–95

Lindsay C, Zhu J, Miller A E, Kirchner P and Wilson T L 2015 Deriving snow cover metrics for Alaska from MODIS *Remote Sens.* **7** 12961–85

Loe L E *et al* 2016 Behavioral buffering of extreme weather events in a high-Arctic herbivore *Ecosphere* **7** 1–13

Marks D, Kimball J, Tingey D and Link T 1998 The sensitivity of snowmelt processes to climate conditions and forest cover during rain-on-snow: a case study of the 1996 Pacific Northwest flood *Hydrol. Process.* **12** 1569–87

Martinaitis S M, Cocks S B, Qi Y, Kaney B T, Zhang J and Howard K 2015 Understanding winter precipitation impacts on automated gauge observations within a real-time system *J. Hydrometeorol.* **16** 2345–63

McCabe G, Clark M and Hay L 2007 Rain-on-snow events in the western United States *Bull. Am. Meteorol. Soc.* **March** 319–28

Merenti-Valimaki H-L 2001 Present weather: comparing human observations and one type of automated sensor *Meteorol. Appl.* **8** 491–6

O'Neel S *et al* 2015 Icefield-to-ocean linkages across the northern Pacific coastal temperate rainforest ecosystem *Bioscience* **65** 499–512

Overland J E and Wang M 2010 Large-scale atmospheric circulation changes are associated with the recent loss of Arctic sea ice *Tellus* **62A** 1–9

Oyler J W, Ballantyne A, Jencso K and Running S W 2015 Creating a topoclimatic daily air temperature dataset for the conterminous United States using homogenized station data and remotely sensed land skin temperature *Int. J. Climatol.* **35** 2258–79

Putkonen J and Roe G 2003 Rain-on-snow events impact soil temperatures and affect ungulate survival *Geophys. Res. Lett.* **30** 1–4

Rees A, Lemmetyinen J, Derksen C, Pulliainen J and English M 2010 Remote sensing of environment observed and modelled effects of ice lens formation on passive microwave brightness temperatures over snow covered tundra *Remote Sens. Environ.* **114** 116–26

Rennert J K, Roe G, Putkonen J and Bitz C M 2009 Soil thermal and ecological impacts of rain on snow events in the circumpolar Arctic *J. Clim.* **22** 2302–15

Riseth J Å *et al* 2011 Sámi traditional ecological knowledge as a guide to science: snow, ice and reindeer pasture facing climate change *Polar Rec. Gr. Brit.* **47** 202–17

Semmens K A, Ramage J, Bartsch A and Liston G E 2013 Early snowmelt events: detection, distribution, and significance in a major sub-Arctic watershed *Environ. Res. Lett.* **8** 014020

Serreze M C and Francis J A 2006 The arctic amplification debate *Clim. Change* **76** 241–64

Singh P, Spitzbart G, Hübl H and Weinmeister H W 1997 Hydrological response of snowpack under rain-on-snow events: a field study *J. Hydrol.* **202** 1–20

Stafford J M, Wendler G and Curtis J 2000 Temperature and precipitation of Alaska: 50-year trend analysis *Theor. Appl. Climatol.* **67** 33–44

Sugg J W, Fuhrmann C M, Perry L B, Hall D K and Konrad C E 2017 Sub-regional snow cover distribution across the southern Appalachian mountains *Phys. Geogr.* **38** 105–23

Tedesco M, Derksen C, Deems J S and Foster J L 2015 Chapter 5 remote sensing of snow depth and snow water equivalent *Remote Sensing of the Cryosphere* ed M Tedesco (New York: Wiley) pp 73–99

Thornton P E, Running S W and White M A 1997 Generating surfaces of daily meteorological variables in complex terrain *J. Hydrol.* **190** 214–51

US Geological Survey 2017 2007-2014, National hydrography dataset available on the World Wide Web (http://nhd.usgs.gov) (Accessed: 20 January 2017)

Vuyovich C M, Jacobs J M, Hiemstra C A and Deeb E J 2017 Effect of spatial variability of wet snow on modeled and observed microwave emissions *Remote Sens. Environ.* **198** 310–20

Wang L, Derksen C, Brown R and Markus T 2013 Recent changes in pan-Arctic melt onset from satellite passive microwave measurements *Geophys. Res. Lett.* **40** 522–8

Wang L, Toose P, Brown R and Derksen C 2016 Frequency and distribution of winter melt events from passive microwave satellite data in the pan-Arctic, 1988–2013 *Cryosphere* **10** 2589–602

Wilson R R, Bartsch A, Joly K, Reynolds J H, Orlando A and Loya W M 2013 Frequency, timing, extent, and size of winter thaw–refreeze events in Alaska 2001-2008 detected by remotely sensed microwave backscatter data *Polar Biol.* **36** 419–26

Yi Y, Kimball J S, Rawlins M A, Moghaddam M and Euskirchen E S 2015 The role of snow cover affecting boreal-arctic soil freeze-thaw and carbon dynamics *Biogeosciences* **12** 5811–29